Journal of Materials Chemistry A

Accepted Manuscript

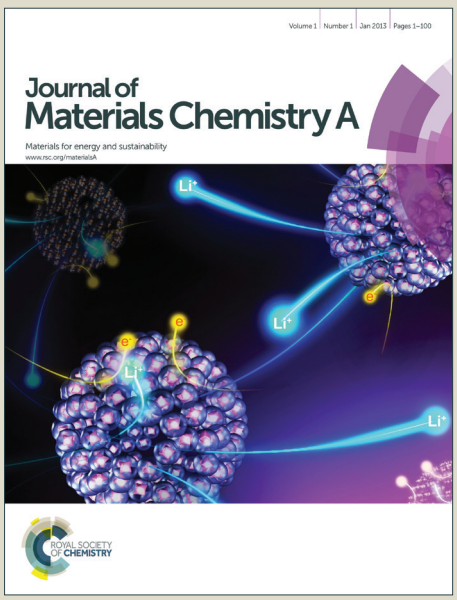

ROYAL SOCIETY OF CHEMISTRY

www.rsc.org/materialsA

Journal of Materials Chemistry A

RSCPublishing

ARTICLE

High performance graphene oxide/polyacrylonitrile composite pervaporation membranes for desalination applications

Cite this: DOI: 10.1039/x0xx00000x

Received 00th January 2012,
Accepted 00th January 2012

DOI: 10.1039/x0xx00000x

www.rsc.org/

Bin Liang[a,†], Wu Zhan[a,†], Genggeng. Qi[b], Sengseng Lin[a], Qian Nan[a], Yuxuan Liu[a], Bing Cao[a,*] and Kai Pan[a,*]

As an emerging technology, pervaporation (PV) has shown great promise in fresh water production from salty water. However, the low separation efficiency of the present membranes hinders their practical applications. Here, thin graphene oxide (GO) films with 2D nanochannels were fabricated on polyacrylonitrile (PAN) ultrafiltration membrane using vacuum filtration-assisted assembly method. The GO/PAN composite membrane exhibit a high water flux up to 65.1 L m^{-2} h^{-1} with high rejection (about 99.8%) for desalination by pervaporation under the 90 ºC. It is noteworthy that the composite membranes show high performance in treating high salinity water even with a salt concentration up to 100,000 ppm. This makes it possible to use GO-based membrane for seawater desalination, brackish water desalination and reverse osmosis concentrate treatment.

1 Introduction

Shortage of water resources is one of the world's most concerning problems. Presently, over a third of the world's population suffer from inadequate safe drinking water.[1,2] Desalination of saltwater, including seawater (a salinity of about 3.5%) and brackish water (a salinity of 0.05-3%), is an important technology for solving the water crisis.[3,4] Among all the desalination applications, Reverse Osmosis (RO) is the major high-efficiency method in producing fresh water at relative low cost.[5-7] However, a high operation pressure is required due to RO separation mechanism.[8] In addition to the plant location and process design restrictions, the typical efficiency of the RO system for desalination is about 35% to 50%, which largely limits the RO productivity. Meanwhile, the concentrated sea water, a byproduct of the process, may also cause a secondary pollution.[9]

To overcome these challenges of RO process, pervaporation, a novel membrane separation technology, has been developed for saltwater desalination. Compared with RO process, pervaporation can be used in desalination for high salinity water beyond RO process can handle. In a typical pervaporation process, a liquid mixture contacts with the pervaporation membrane and desorbs at the permeate side.[10-12] The mass transfer driving force is the chemical potential between the two sides of the membrane, which is related to the difference of the affinity of the membrane to the components and their mass transfer resistance in the membrane. The chemical potential difference is provided by the vacuum or air blow. It has been widely accepted that the major mechanism of the pervaporation process is solution-diffusion which involves three steps: (1) the component is adsorbed and dissolved on the membrane surface; (2) the dissolved component diffuses through the membrane; (3) the component desorbs at the permeate side.[13,14] At present, pervaporation has been widely used in organic solvent dehydration, removal of volatile organic compounds from aqueous feeds and organic mixture separation.[15-18] However, the mass transfer efficiency of most pervaporation membranes currently is still relatively low compared with the RO membranes, which limits its application in practical field.

A key component in design for high performance membrane is the chemical properties of membrane materials. At present, pervaporation membranes were fabricated by different materials, such as polymer material, inorganic material and polymer-inorganic hybrid material (crosslinked PVA, NaA zeolite, and PVA/ maleic acid (MA)/silica, respectively).[19-21] All of these membranes showed good rejection performance for monovalence ions. But the water flux of all the membranes prepared by materials above is generally quite low, no more than 10 L m^{-2} h^{-1}. It has been well known that graphene oxide (GO) is a new, intriguing material due to its ultra-thin 2D structure and multi-functional surface chemistry.[22,23] Due to the fabrication process using acids and strong oxidizers, the surface of GO has a variety of functional groups such as epoxide, carbonyl and hydroxyl groups.[24-26] Because of their unique transport properties, GO nanosheets have attracted intensive interests in the field of membrane applications.[27-29] GO has been used as a starting material for preparation of thin films, paper-like materials or membranes.[30-33] Many efforts have been made to fabricate highly permeable GO-based membranes by taking advantage of the fast water transport along the nanochannels between graphene sheets.[34-36]

While desalination via nanofiltration, reverse osmosis and organic dehydration by pervaporation have been studied,[37-39] there is no report for pervaporation desalination using GO-based membranes. In

the present work, using a facile vacuum filtration-assisted assembly method we fabricated the pervaporation composite membranes by depositing GO films with 2D nanochannels on a functionalized polyacrylonitrile (PAN) ultrafiltration membrane. These GO/PAN composite membranes show great potential for desalination applications by pervaporation. Under our testing conditions these pervaporation composite membranes exhibit a high water flux up to 65.1 L m^{-2} h^{-1} with high rejection for desalination (about 99.8% under the 90 ºC). It is noteworthy that the composite membranes retain high performance in treating high salinity water even with a salt concentration up to 100,000 ppm.

2 Experimental

2.1 Materials

Graphite powder (40 μm) was purchased from Qingdao Henglide Graphite Co., Ltd. Commercial PAN ultrafiltration membrane (molecule cutoff 40 W) used as the matrix to support the GO layer was purchased from company (Ande Membrane Inc., China). All of the water used in this work was Milli-Q deionized water (18.1 MΩ cm at 25 ºC).

2.2 Preparation of GO aqueous suspensions

Modified Hummers' method[40] was applied to prepare the GO aqueous suspensions (see Supporting Information). The resulting GO aqueous dispersion (1.23 g L^{-1}) was sonicated for 30 min followed by centrifugation at 10,000 rpm for 30 min to obtain a homogeneous dispersed aqueous suspensions. Then the GO suspensions were diluted to 100 mg L^{-1} and 10 mg L^{-1} for the fabrication of GO layer.

2.3 Preparation of GO/PAN composite membrane

Commercial PAN ultrafiltration membrane was firstly immersed into NaOH solution (1 M) at 60 ºC for 2 h to modify the membrane surface by a hydrolysis process. GO/PAN composite membranes were prepared by vacuum filtration of the aforesaid GO suspensions (10 and 100 mg L^{-1}) through modified PAN ultrafiltration membrane.

2.4 Characterization of GO and GO/PAN composite membranes

ATR-FTIR spectra were obtained on a Perkin-Elmer Spectrum 2000 FTIR instrument (USA). XRD was carried out on an X' Pert PRO diffractometer equipped with Cu Ka radiation (40 kV, 40 mA). TEM studies were conducted on a JEOL JEM 2010 electron microscope at 200 kV. The TEM samples are prepared by placing a drop of diluted dispersion onto holey carbon grids. TGA was carried out on a Perkin-Elmer Pyris 6 TGA instrument under nitrogen with a heating rate of 10 ºC min^{-1}. XPS measurements were carried out on a Kratos Axis Ultra DLD instrument equipped with a monochromated Al Ka x-ray source and hemispherical analyzer capable of an energy resolution of 0.5 eV. Raman measurements were conducted on a LabRam-1B Raman spectroscope equipped with a 633 nm laser source. The contact angle measurements were carried out on a JC 2000 (MAIST Vision Inspection & Measurement Ltd. Co.). SEM images were obtained by Hitachi S-4700 field-emission SEM system.

2.5 Pervaporation desalination measurements

The pervaporation separation process was performed following the Solution-Diffusion model, where the feed solution directly contacts with the membrane, gets dissolved onto the membrane surface, diffuses through the membrane, and then evaporates. The vapor stream leaving the membrane is passed through a condenser, and the liquid collected is called "permeate". The performance of the GO/PAN composite membranes for desalination with different concentrations of NaCl solution were measured at different temperatures. The flux was determined by dividing the weight of the collected permeate by the product of the membrane effective area and the sampling time. The concentration of feed solution and permeate were determined using conductivity meter (Oakton® Con 110, China). The detailed description of pervaporation measurements can be found in our previous work.[19]

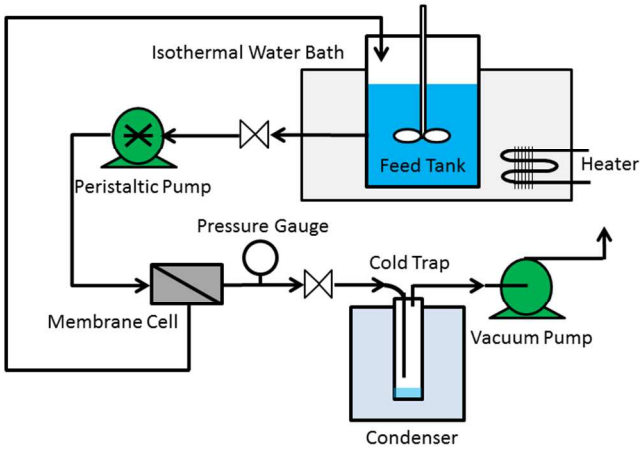

Fig. 1 Schematic diagram of the pervaporation unit.

Pervaporation experiments were carried out using a laboratory scale pervaporation unit as shown in Fig. 1. The membrane was placed in the middle of a pervaporation cell and the effective surface area of the membrane of 14.7 cm^2. NaCl aqueous solutions with different concentrations were used as the feed solutions. During the experiment, the feed solution was preheated in a water bath to the required temperature and pumped to the pervaporation cell using a Langer® peristaltic pump. The pressure on the permeate side of the membrane cell was maintained at 100 Pa. The permeate was collected in a liquid nitrogen cold trap.

The pervaporation desalination performance of composite membranes was evaluated by measuring water flux and salt rejection. The water flux (J) was determined from the mass (M) of the permeate collected in the cold trap, the effective membrane area (A) and the experimental time (t) using the following equation:

$$J = \frac{M}{A \times t} \quad (1)$$

The salt concentrations of the feed (C_f) and the permeate (C_p) were determined from the conductivity measured with an Oakton® Con 110 conductivity meter. The conductivity meter was calibrated using standard NaCl solutions with different concentrations from 0-100,000 ppm. A calibration curve was then constructed. The salt rejection (R) was determined by the following equation:

$$R = \frac{C_f - C_p}{C_f} \times 100\% \quad (2)$$

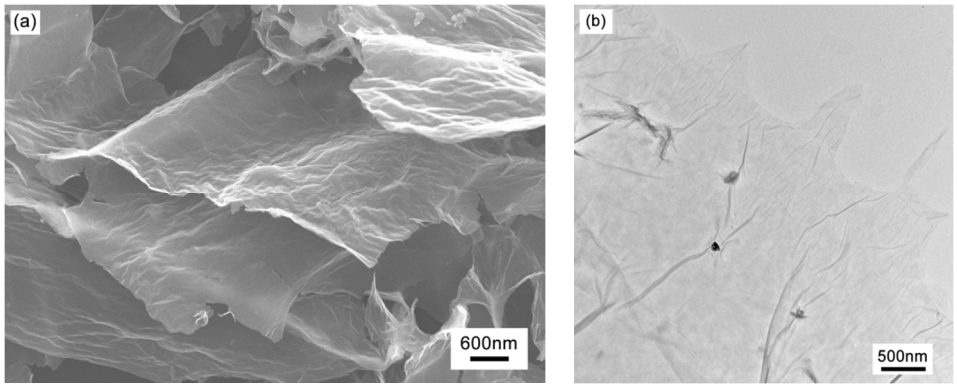

Fig. 2 (a) SEM and (b) TEM morphology of the GO sample.

The permeate side of the membrane cell was flushed with deionized water after 10 h and the conductivity of the stream was measured to check for salt leaking or crystallization. In the whole study, the GO/PAN composite membranes were clean and no salt precipitation or crystallization on the permeate side of the membrane was observed.

3 Results and discussion

3.1 Characterization of GO structures

Field emission scanning electron microscopy (FESEM) and transmission electron microscopy (TEM) were used to characterize the nanoscale morphology of the GO samples prepared following the modified Hummer's method. From the SEM images in Fig. 2 (a) and Fig. S1 (a), exfoliated GO thin flakes with wavy wrinkles were found. Fig. 2 (b) and Fig. S1 (b) show the TEM images of GO samples. The GO sheets have a shape similar to large crumpled thin flakes, in consistent with the SEM results.[41,42]

The attenuated total reflectance-fourier transform infrared (ATR-FTIR) spectrum of the GO barrier layer (Fig. 3 (a)) indicates the presence of hydroxyl, carboxyl and epoxide functional groups (i.e., -OH at 3430 cm^{-1}, -COO- at 1720 cm^{-1}, unoxidized sp2 -C=C- bonds in the carbon lattice at 1635 cm^{-1},[43,44] -C-OH stretching at 1230 cm^{-1}, and -C-O-C- stretching at 1072 cm^{-1}) resulted from the oxidation process, leading to the hydrophilic nature of GO.[45,46] From the thermogravimetric analysis (TGA) measurement, GO shows a great weight loss about 39.3 % before 250 ºC (Fig. 3 (b)). One main peak at 2θ= 12.02º was observed in the X-ray diffraction (XRD) pattern of GO (Fig. 3 (c)). The calculated average interlayer spacing of the GO

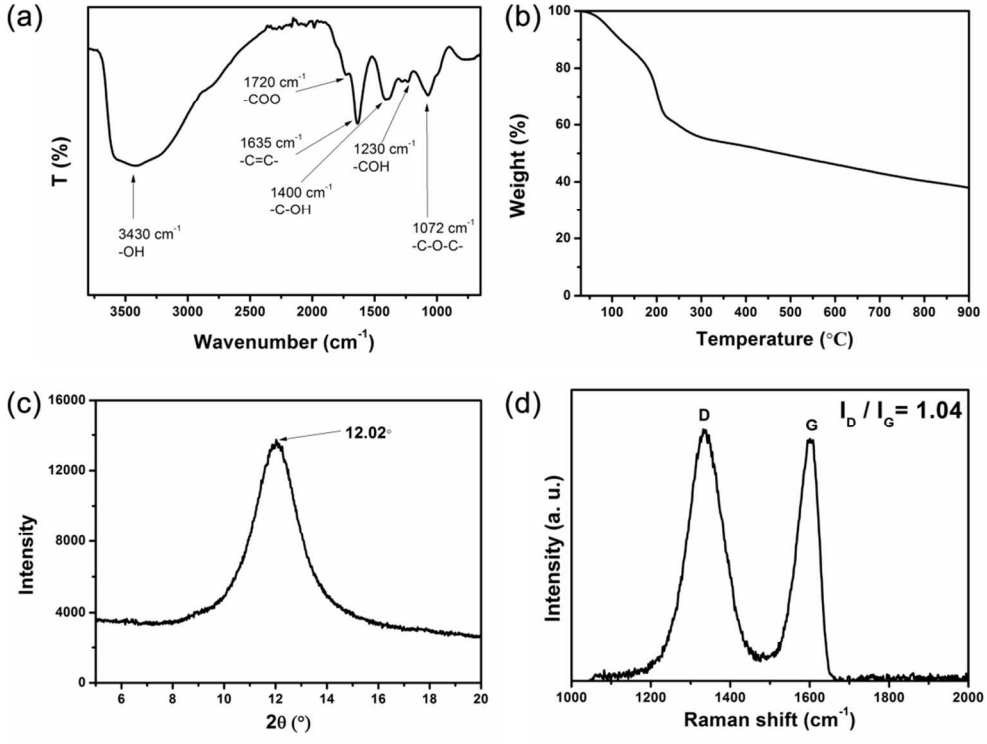

Fig. 3 Characterization of GO nanosheets: (a) ATR-FTIR; (b) TGA; (c) XRD and (d) Raman shift.

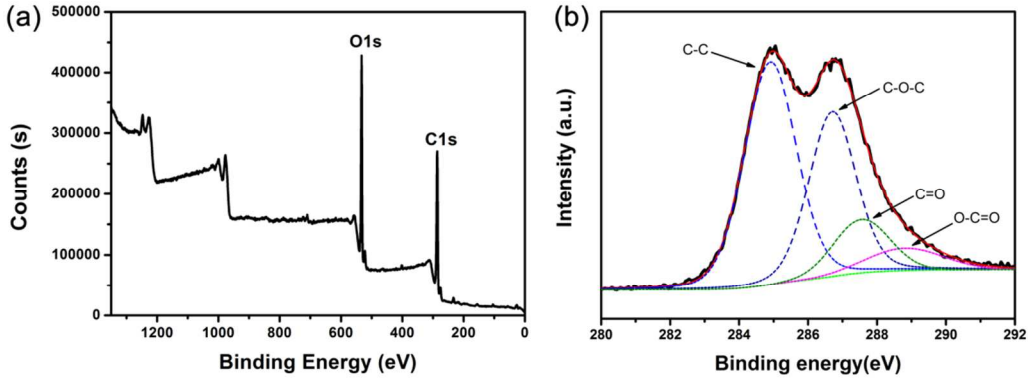

Fig. 4 Surface chemistry of GO sample: (a) XPS spectrum and (b) XPS deconvolution results of the C1s spectrum.

films is 7.36 Å. The Raman spectrum of the GO films shows the characteristic G and D bands (1590 and 1340 cm^{-1}, respectively) of carbon materials, which are related to the graphitized structure and local defects/disorders particularly located at the edges of graphene and graphite platelets, respectively.[47] Therefore, a lower I_D/I_G peak intensity ratio suggests fewer defects or disorders in the graphitized structure. From the Raman spectrum in Fig. 3 (d), the ratio of the I_D/I_G is 1.04, which is similar to those of GO films in previous studies.[45,47]

The results of X-ray photoelectron spectroscopy (XPS) characterization show that the elementary composition of GO sheets (Fig. 4 (a)). The C/O molar ratio determined for the GO sheets is 2.49. The XPS fitting data (Fig. 4 (b)) suggest the presence of C–C/C=C groups (283.9 eV), C–O groups (286.7 eV), C=O groups (287.6 eV), and O–C=O groups (288.9 eV) with atomic percentages of 48.2%, 37.2%, 11.6% and 3.0%, respectively. The XPS results above agree well with the Lerf-Klinowski Model of GO, as shown in Fig. 5.[48]

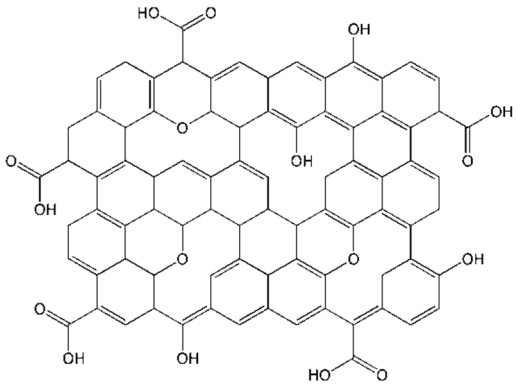

Fig. 5 The Lerf-Klinowski Model of the GO nanosheet structure.

3.2 Microstructure of GO/PAN composite membranes

The topographic and cross-section morphology of the GO/PAN membranes are characterized by SEM, as depicted in Fig. 6 (b) and (c). The PAN membrane consists of some nanopores at the upper surface and macroporous voids at the lower cross-section. The densely stacked GO films shows a good affinity to the modified PAN film (Fig. 6 (c)) so that they did not peel off from the modified PAN substrate (Fig. 6 (a)), which is possibly resulted from the strong hydrogen bonds between the -COOH or -$CONH_2$ groups of modified PAN and the GO hydroxyl and carboxyl groups.[49]

3.3 Pervaporation performance of membranes on desalination

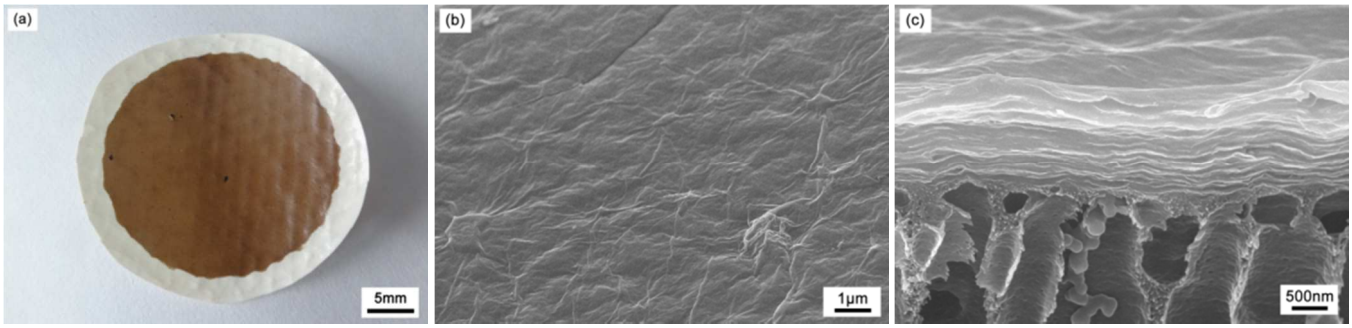

Fig. 6 Morphology of the GO/PAN composite membrane: (a) digital photo; (b) SEM images of the surface and (c) cross-section of the membrane.

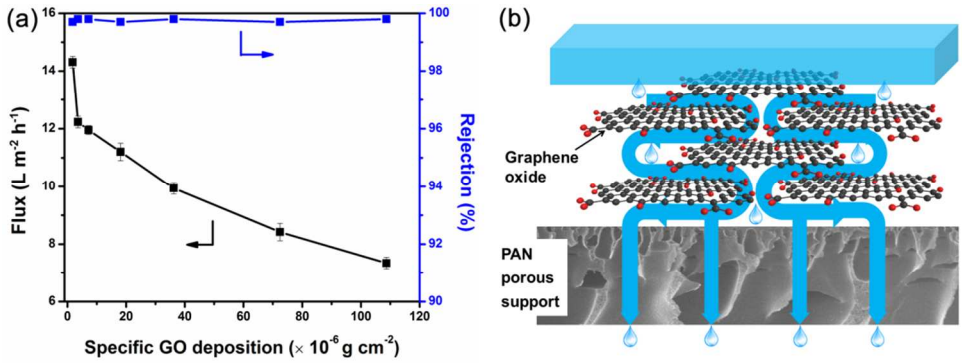

Fig. 7 (a) Effects of specific GO deposition amount on the pervaporation performance of GO/PAN membranes and (b) Schematic representation of the mechanism for water molecule transport through GO sheet.

It is well known that PAN ultrafiltration membrane can hardly reject salt ions. A series of GO/PAN composite membranes with different loadings of GO, ranging from 1.8 to 115.9 μg cm^{-2} (Fig. 7 (a)) were fabricated to evaluate the effect of specific GO deposition on water transportation performance at 30 ºC. The GO film thickness increases linearly with the specific GO deposition (Fig. S2). Increasing the specific GO deposition from 1.8×10^{-6} g cm^{-2} to 115.9×10^{-6} g cm^{-2} resulted in an increase in the film thickness from 30 to 1400 nm. At a specific GO deposition of 1.8×10^{-6} g cm^{-2}, the GO film deposited on the substrate is rather transparent. It turned opaque with a blackish brown color at a higher deposition of 3.6×10^{-6} g cm^{-2}. The inset pictures in Fig. S3 also demonstrate the flexibility of the GO film, as the GO/PAN membranes can endure extensive bending without cracking the GO film. The fluxes were recorded until a steady state was reached, typically after half an hour. The highest steady flux up to 14.3 L m^{-2} h^{-1} was reached at a GO loading of about 1.8 μg cm^{-2}. As shown in Fig. 7 (a), a significant decrease in the water flux was observed with increasing GO loading above 5 μg cm^{-2}, which could be due to the higher mass transfer resistance as the transport path of water molecules are increased with thicker deposition of the GO films. In general, as the mass transfer resistance increases, the membrane efficiency drops.[21,50] However, the rejection of the GO/PAN composite membrane maintained over 99.7% with increasing thickness of the GO layers. Therefore, minimizing the thickness of the GO layer while maintaining its structural integrity is the key in fabricating high efficiency pervaporation membranes. We assumed that, as illustrated in Fig. 7 (b), the "ideal" pathway for water molecules transport through the tortuous nano-capillaries between the well stacked GO sheets,[34,51,52] where the GO inter-sheet spacing determines the selectivity performance of membrane.

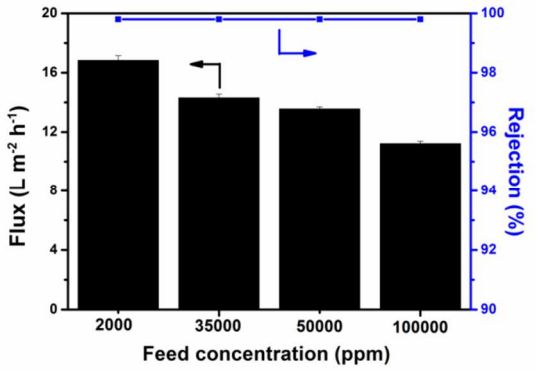

Fig. 8 Effects of feed concentration on the pervaporation performance of GO/PAN membrane.

The pervaporation desalination performances of the composite membrane were evaluated. Fig. 8 showed the effect of salt concentration in the feed solution on the separation performance of the GO/PAN membrane at 30 ºC. In general, the water permeate flux decreased as the solute concentration increased. The flux for 2000, 35,000, 50,000 and 100,000 ppm NaCl solutions was 16.84, 14.31, 13.56 and 11.23 L m^{-2} h^{-1}, respectively. The corresponding values for salt rejection were 99.8%, 99.8%, 99.8% and 99.8%, respectively. An aqueous salt solution can be regarded as a pseudo-liquid mixture containing free water molecules and bulkier hydrated ions formed in solution. As the salt concentration increased from 2,000 to 100,000 ppm, the water concentration decreased from 99.8 to 90.0 wt%.

Table 1 Pervaporation performance of the membrane skin layer prepared by different materials

Material	Feed concentration (ppm)	T (°C)	Flux (L m^{-2} h^{-1})	Rejection (%)
Polyether amide[53]	35,000	68-70	0.2	>99.9
Polyether ester[54]	5,200	22-29	0.15	>99
NaA zeolite[20]	35,000	69	1.9	>99.9
PVA/MA/Silica[21]	20,00	22	6.93	>99.5
PVA/GA[19]	35,000	25	7.36	>99.8
GO (this study)	35,000	30	14.3	>99.8
GO (this study)	35,000	90	65.1	>99.8

Although the diffusion in the membrane is concentration independent, the adsorption of feed solution components at the interface between feed solution and membrane is affected directly by the feed concentration. Therefore, the concentration of hydrated ions on the membrane will increase with the increase of feed solution and thus decrease of water flux. In the other hand, the occurrence of increased concentration polarization with an increase in solute concentration adjacent to membrane surface may also cause the decrease in the water flux

The pervaporation performance of the membranes prepared with different materials was also examined. As shown in Table 1, the composite membrane prepared with a GO skin layer exhibited a better separation performance compared with the membrane prepared using other materials.

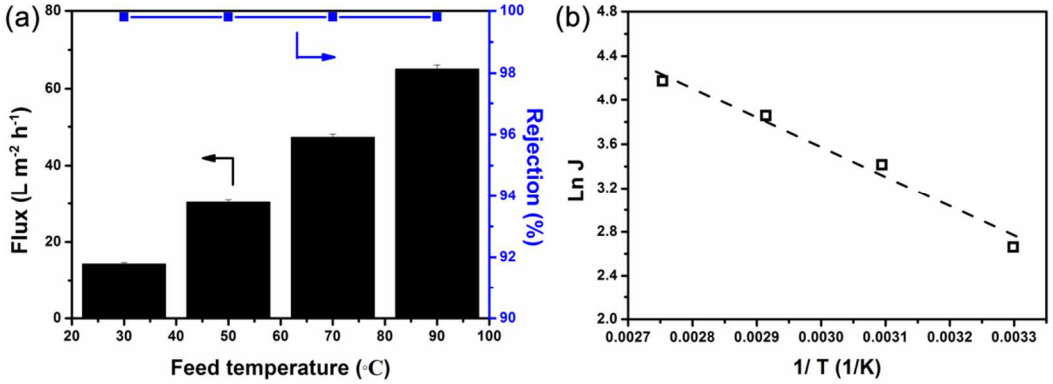

Fig. 9 (a) Effects of feed temperature on the pervaporation performance of GO/PAN membrane and (b) the Arrhenius plot of the water flux and feed temperature.

Fig. 9 (a) shows the effect of the feed temperature on the pervaporation desalination performance of the GO/PAN composite membrane with a GO layer thickness of 100 nm at a vacuum of 100 Pa. For all feed concentrations, there was an exponential increase in water flux when the feed temperature increased from 30 to 90 ºC. A high water flux of 65.1 L m^{-2} h^{-1} was achieved at a feed temperature of 90 ºC. This is not surprising, because the driving force for the pervaporation process is the partial vapor pressure difference between the feed and the permeate. As the feed temperature increased, the water vapor pressure on the feed side increased exponentially while the vapor pressure on the permeate side did not change, and therefore the driving force increased leading to the increase of water flux.

The temperature dependence of the permeate flux for pervaporation generally follows an Arrhenius type relationship:[55]

$$J_i = A_i \exp(-\frac{E_{p,i}}{RT}) \quad (3)$$

where J_i is the permeate flux of membrane, A_i is the pre-exponential factor, R is the gas constant, T is the absolute temperature and $E_{p,i}$ is the apparent activation energy for permeation, which depends on both the activation energy for diffusion and the heat of sorption. Fig. 9 (b) shows the Arrhenius plot of the water flux and feed temperature. The results show that the water flux and the reciprocal of the absolute temperature of the feed follow a linear relationship. The activation energy of water permeation ($E_{p,w}$) through the membrane was taken from the slope of the Arrhenius plot (Eq. (3)). And the activation energy of water permeation is about 22.19 kJ mol^{-1}. The positive value of $E_{p,w}$ suggests that water flux should increase with increasing temperature. The relatively low activation energy could be attributed to the unique structure of GO film. Water molecules can diffuse through the space between GO sheets easily. Therefore, the activation energy is low.

4 Conclusions

In summary, a thin GO film has been prepared on modified PAN ultrafiltration membrane by vacuum filtration-assisted assembly method. The morphology of the GO film reveals a well-packed structure with a layer-by-layer pattern. Pervaporation performance indicates that the GO film exhibits preferential water transport with particularly high water permeability and salt rejection for salty water with different concentrations. The GO/PAN composite membranes exhibit a high water flux up to 65.1 L m^{-2} h^{-1} with high rejection (about 99.8%) for desalination by pervaporation under the 90 ºC. It is noteworthy that the composite membranes show high performance in treating high salinity water even with a salt concentration up to 100,000 ppm. This makes it possible to use GO-based membrane by pervaporation for seawater desalination, brackish water desalination and reverse osmosis concentrate treatment.

Acknowledgements

This project was supported by the National Natural Science Foundation of China (51373014), and the Opening Project of the State Key Laboratory of Chemical Resource Engineering (CRE-2012-C-206).

Notes and references

[a] Key laboratory of carbon fiber and functional polymers, Ministry of Education, Beijing University of Chemical Technology, Beijing 100029, China.

[b] Department of Materials Science and Engineering, Cornell University, Ithaca, NY, USA.

† Author Contributions

These authors contributed equally to this work.

Corresponding author

Tel.: 86-10-64413857
E-mail: pankai@mail.buct.edu.cn (Kai Pan); bcao@mail.buct.edu.cn (Bing Cao).

Electronic Supplementary Information (ESI) available: [SEM and TEM images characterizing the morphology of the GO sample, SEM and digital photos characterizing the GO film thickness with different specific GO depositions; Digital photos characterizing folding GO/PAN composite membrane.]. See DOI: 10.1039/b000000x/

References

1 M. Elimelech and W. A. Phillip, *Science*, 2011, **333**, 712-717.
2 R. L. McGinnis and M. Elimelech, *Environ. Sci. Technol.*, 2008, **42**, 8625-8629.
3 R. F. Service, *Science*, 2006, **313**, 1088-1090.
4 R. J. Singh, *J. Membr. Sci.*, 2008, **313**, 353-354.
5 S. Kasemset, A. Lee, D. J. Miller, B. D. Freeman and M. M. Sharma, *J. Membr. Sci.*, 2013, **425-426**, 208-216.
6 B. J. Feinberg, G. Z. Ramon and E. M. V. Hoek, *Environ. Sci. Technol.*, 2013, **47**, 2982-2989.
7 D. Li and H. T. Wang, *J. Mater. Chem.*, 2010, **20**, 4551-4566.
8 L. F. Greenlee, D. F. Lawler, B. D. Freemana, B. Marrot and P. Moulin, *Water Res.*, 2009, **43**, 2317-2348.
9 H. J. Wang, S. B. Ding, H. L. Zhu, F. Wang, Y. H. Guo, H. P . Zhang and J. Y. Chen, *Sep. Purif. Technol.*, 2014, **126**, 82-94.
10 L. Y. Jiang, Y. Wang, T.-S. Chung, X. Y. Qiao and J.-Y. Lai, *Prog. Polym. Sci.*, 2009, **34**, 1135-1160.
11 M. Drobek, C. Yacou, J. Motuzas, A. Julbe, L. P. Ding and J. C. Diniz da Costa, *J. Membr. Sci.*, 2012, **415-416**, 816-823.
12 B. Cao and M. A. Henson, *J. Membr. Sci.*, 2002, **197**, 117-146.
13 A. D. Berloa, I. F. J. Vankelecom and B. V. Bruggen, *J. Membr. Sci.*, 2011, **374**, 138-149.
14 P. Shao and R.Y.M. Huang, *J. Membr. Sci.*, 2007, **287**, 162-179.
15 V. T. Magalad, G. S. Gokavi, M. N. Nadagouda and T. M. Aminabhavi, *J. Phys. Chem. C*, 2011, **115**, 14731-14744.
16 Q. Liu, B. X. Huang and A. S. Huang, *J. Mater. Chem. A*, 2013, **1**, 11970-11974.
17 J. Li, S. L. Ji, G. J. Zhang and H. X. Guo, *Langmuir*, 2013, **29**, 8093-8102.
18 A. V. Talyzin, T. Hausmaninger, S. J. You and T. Szabó, *Nanoscale*, 2014, **6**, 272-281.
19 B. Liang, K. Pan, L. Li, E. P. Giannelis and B. Cao, *Desalination*, 2014, **347**, 199-206.
20 C. H. Cho, K.Y. Oh, S. K. Kim, J. G. Yeo and P. Sharma, *J. Membr. Sci.*, 2011, **371**, 226-238.
21 Z. Xie, M. Hoang, T. Duong, D. Ng, B. Dao and S. Gray, *J.Membr. Sci.*, 2011, **383**, 96-103.
22 F. Kim, L. J. Cote and J. X. Huang, *Adv. Mater.*, 2010, **22**, 1954-1958.
23 Y. J. Song, K. G. Qu, C. Zhao, J. S. Ren and X. G. Qu, *Adv. Mater.*, 2010, **22**, 2206-2210.
24 J. Kim, L. J. Cote, F. Kim, W. Yuan, K. R. Shull and J. X. Huang, *J. Am. Chem. Soc.*, 2010, **132**, 8180-8186.
25 H. K. He, and C. Gao, *Chem. Mater.*, 2010, **52**, 5054-5064.
26 Y. W. Zhu, S. Murali, W. W. Cai, X. S. Li, J. W. Suk, J. R. Potts and R. S. Ruoff, *Adv. Mater.*, 2010, **22**, 3906-3924.
27 B. G. Choi, Y. S. Huh, Y. C. Park, D. H. Jung, W. H. Hong and H. S. Park, *Carbon*, 2012, **50**, 5395-5402.
28 Y. M. Lee, B. Jung, Y. H. Kim, A. R. Park, S. Han, W.-S. Choe and P. J. Yoo, *Adv. Mater.*, 2014, **26**, 3899-3904.
29 J. Lee, H.-R. Chae, Y. J. Won, K. Lee, C.-H. Lee, H. H. Lee, I.-C. Kim, J.-M. Lee, *J. Membr. Sci.*, 2013, **448**, 223-230.
30 Y.-H. Yang, L. Bolling, M. A. Priolo and J. C. Grunlan, *Adv. Mater.*, 2013, **25**, 503-508.
31 Ravikumar and K. Scott, *Chem. Commun.*, 2012, **48**, 5584-5586.
32 M. R. Karim, K. Hatakeyama, T. Matsui, H. Takehira, T. Taniguchi, M. Koinuma, Y. Matsumoto, T. Akutagawa, T. Nakamura, S.-I. Noro, T. Yamada, H. Kitagawa and S. Hayami, *J. Am. Chem. Soc.*, 2013, **135**, 8097-8100.
33 I. Akin, E. Zor, H. Bingol and M. Ersoz, *J. Phys. Chem. B*, 2014, **118**, 5707-5716.
34 D. W. Boukhvalov, M. I. Katsnelson and Y.-W. Son, *Nano Lett.*, 2013, **13**, 3930-3935.
35 D. Cohen-Tanugi and J. C. Grossman, *Nano Lett.*, 2012, **12**, 3602-3608.
36 Y. P. Tang, D. R. Paul and T. S. Chung, *J. Membr. Sci.*, 2014, **458**, 199-208.
37 Y. Han, Z. Xu and C. Gao, *Adv. Funct. Mater.*, 2013, **23**, 3693-3700.
38 W. Choi, J. Choi, J. Bang and J.-H. Lee, *ACS Appl. Mater. Interfaces*, 2013, **5**, 12510-12519.
39 J. Zuo and T.-S. Chung, *J. Mater. Chem. A*, 2013, **1**, 9814-9826.
40 K. Hu, M. K. Gupta, D. D. Kulkarni and V. V. Tsukruk, *Adv. Mater.*, 2013, **25**, 2301-2307.
41 K. A. Mkhoyan, A. W. Contryman, J. Silcox, D. A. Stewart, G. Eda, C. Mattevi, S. Miller and M. Chhowalla, *Nano Lett.*, 2009, **9**, 1058-1063.
42 Z. T. Luo, Y. Lu, L. A. Somers and A. T. C. Johnson, *J. Am. Chem. Soc.*, 2009, **131**, 898-899.
43 C. Bao, Y. Guo, B. Yuan, Y. Hu and L. Song, *J. Mater. Chem.*, 2012, **22**, 23057-23063.
44 N. A. Travlou, G. Z. Kyzas, N. K. Lazaridis and E. A. Deliyanni, *Langmuir*, 2013, **29**, 1657-1668.
45 T.-M. Yeh, Z. Wang, D. Mahajan, B. S. Hsiao and B. Chu, *J. Mater. Chem. A*, 2013, **1**, 12998-13003.
46 Y. Feng, N. Feng and G. Du, *RSC Adv.*, 2013, **3**, 21466-21474.
47 H. Li, Z. N. Song, X. J. Zhang, Y. Huang, S. G. Li, Y. T. Mao, H. J. Ploehn, Y. Bao and M. Yu, *Science*, 2013, **342**, 95-98.
48 D. R. Dreyer, S. Park, C. W. Bielawski and R. S. Ruoff, Chem. *Soc. Rev.*, 2010, **39**, 228-240.
49 W.-S. Hung, C.-H. Tsou, M. D. Guzman, Q.-F. An, Y.-L. Liu, Y.-M. Zhang, C.-C. Hu, K.-R. Lee and J.-Y. Lai, *Chem. Mater.*, 2014, **26**, 2983-2990.
50 S. C. George and S. Thomas, *Prog. Polym. Sci.*, 2001, **26**, 985-1017.
51 C. Xu, A. J. Cui, Y. L. Xu and X. Z. Fu, *Carbon*, 2013, **62**, 465-471.
52 W.-S. Hung, Q.-F. An, M. D. Guzman, H.-Y. Lin, S.-H. Huang, W.-R. Liu, C.-C. Hu, K.-R. Lee, J.-Y. Lai, *Carbon*, 2014, **68**, 670-677.
53 H. J. Zwijnenberg, G. H. Koops and M. Wessling, *J. Membr. Sci.*, 2005, **250**, 235-246.
54 E. Quiñones-Bolaños, H. D. Zhou, R. Soundararajan and L. Otten, *J. Membr. Sci.*, 2005, **252**, 19-28.

55 F. B. Peng, L. Y. Lu, H. L. Sun and Z. Y. Jiang, *J. Membr. Sci.*, 2006, **281**, 600-608.

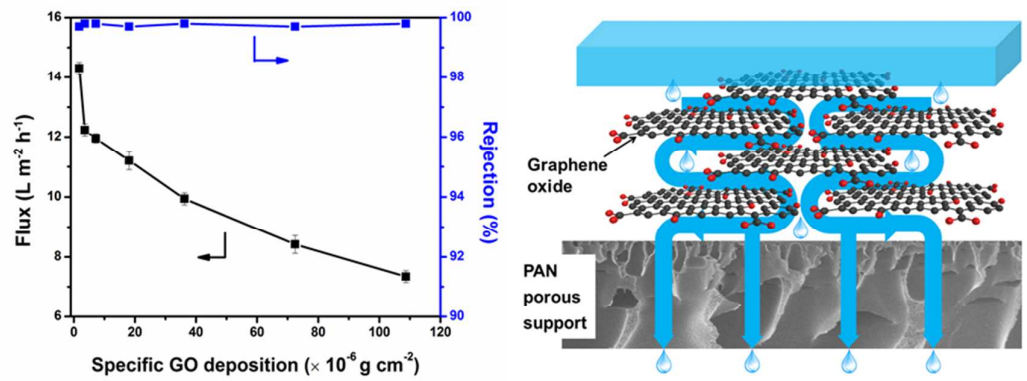

A GO/PAN pervaporation composite membrane was prepared for desalination with high performance.